Targeted Micro-Robots Locate Cancer Cells

Ruijie He[a,b], Shenglan Yuan[a,*]

[a]Department of Mathematics, School of Sciences, Great Bay University, Dongguan 523000, China
[b]School of Mathematics,Sun Yat-sen University, Guangzhou 510275, China

Abstract

Keywords:

1. Introduction

This work is to address how targeted micro-robots carrying drugs locate cancer cells, we present a mathematical model based on chemotaxis-driven movement and ligand-receptor binding. The model consists of three key equations describing the chemoattractant concentration, free micro-robots, and bound micro-robots.

2. Mathematical model

We are going to model the targeted delivery of drugs by micro-robots to cancer cells. The key steps include three parts. The release of micro-robots in the bloodstream. The navigation of micro-robots towards the tumor site, which we assume is guided by a chemical gradient (chemotaxis) or other targeting mechanisms. The binding of micro-robots to cancer cells.

We will focus on chemotaxis as a primary mechanism. The mathematical model will involve diffusion of chemoattractants (chemical signals) from the tumor, movement of micro-robots towards higher concentrations of chemoattractants, and binding kinetics when micro-robots come in contact with cancer cells. We will model the system using partial differential equations (PDEs) for the chemoattractant concentration and the density of micro-robots.

The chemoattractant is produced by the tumor cells. We model its diffusion and decay:

$$\frac{\partial c}{\partial t} = D_c \nabla^2 c - kc + S(\mathbf{x}),$$

where $c(\mathbf{x}, t)$ is the concentration of chemoattractant at position $\mathbf{x}$ and time t, D_c is the diffusion coefficient (0.1 mm^2/s) of the chemoattractant, ∇^2 is the Laplacian operator in 3D, k is the decay rate (0.01 s^{-1}), and $S(\mathbf{x})$ is the tumor source term located at some region (1.0 nM/s in tumor region).

The micro-robots move by chemotaxis and diffuse randomly due to blood flow and other factors. The equation for the free micro-robots (movement via chemotaxis) is

$$\frac{\partial \rho}{\partial t} = D_\rho \nabla^2 \rho - \nabla \cdot (\chi \rho \nabla c) - k_b \rho \delta_{\Omega_T} + k_u b,$$

where $\rho(\mathbf{x}, t)$ is the density of micro-robots at position x and time t, D_ρ is the diffusion coefficient (0.01 mm^2/s) of micro-robots, ∇ is the gradient operator in 3D, χ is the chemotactic sensitivity (0.1 $\text{mm}^2/\text{nM}\cdot\text{s}$), k_b is the binding rate (0.1 s^{-1}) to cancer cells (only in the tumor region Ω_T), k_u is the unbinding rate (0.01 s^{-1}) since we assume bound

*Corresponding author
Email addresses: gravitas_sysu@qq.com (Ruijie He), shenglanyuan@gbu.edu.cn (Shenglan Yuan)

micro-robots can detach at a low rate, and δ_{Ω_T} is the indicator function that equals to 1 inside tumor region Ω_T, 0 otherwise.

The bound micro-robots attached to cancer cells satisfy

$$\frac{\partial b}{\partial t} = k_b \rho \delta_{\Omega_T} - k_u b,$$

where $b(\mathbf{x}, t)$ the density of bound micro-robots.

3. Numerical simulations

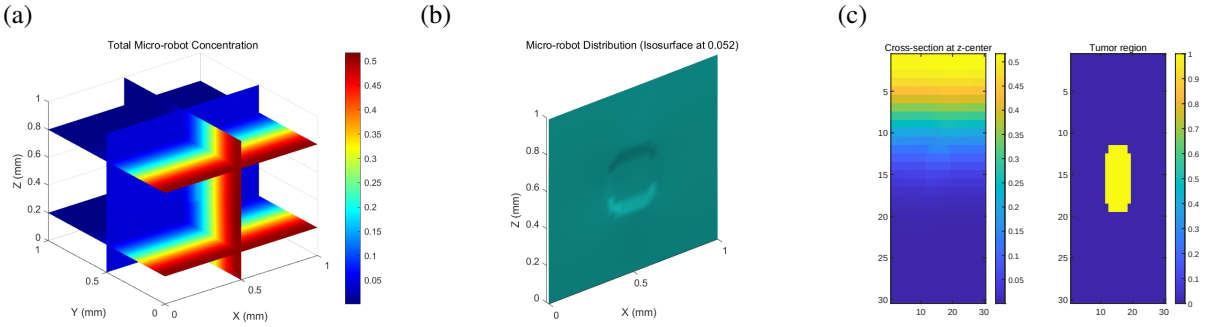

Figure 1: (a) Cross-sections of total robot concentration; (b) 3D surface at 10% of max concentration; (c) 2D slices through domain center.

Figure 1 simulates a 3D chemotaxis-driven micro-robot drug delivery system. The simulation is configured within a 1 mm^3 spatial domain, discretized with a grid of 30 points along each dimension. To ensure numerical stability, a time step of 0.001 seconds is used, and the total simulated time is 2 seconds. The key biochemical parameters governing the system include diffusivities for the chemoattractant and micro-robots ($D_c = 0.1$ and $D_\rho = 0.01$, respectively), a chemotactic sensitivity of $\chi = 0.1$, and binding/unbinding rates of $k_b = 0.2$ and $k_u = 0.01$. The environment is initialized with a tumor modeled as a spherical region at the center with a radius of 0.15 mm, which acts as a continuous source of chemoattractant. The population of micro-robots is introduced into the system via an initial injection across the entire plane at $x = 0$. At each time step of the simulation loop, zero-flux Neumann boundary conditions are enforced to contain all elements within the modeled domain. The chemoattractant field is updated by calculating its diffusion, incorporating a constant production term from the central tumor, and subtracting a natural decay term. Concurrently, the micro-robot population undergoes movement driven by a combination of random diffusion and a directed chemotactic velocity proportional to the spatial gradient of the chemoattractant (∇c), guiding them toward higher concentrations. Binding and unbinding kinetics, governed by their respective rates, are exclusively calculated for micro-robots located within the tumor region. Finally, after all updates are computed, the concentrations of all species are clipped to ensure non-negativity, maintaining physical realism before proceeding to the next iteration. We compute the 3D Laplacian using central differences, calculate the chemotaxis term $\nabla \cdot (\rho \nabla c)$, and implement zero-flux boundaries by copying adjacent grid values. Visualization of the simulation data is achieved through multiple complementary methods. A slice plot provides a cross-sectional view of the total micro-robot concentration, revealing internal gradients within the volume in Figure 1(a). To render the three-dimensional structure of the robot swarm, an isosurface is generated at a threshold of 10% of the maximum concentration in Figure 1(b). Finally, for detailed quantitative analysis, 2D cross-sectional slices are extracted through the center of the domain and overlaid with a tumor mask to clearly distinguish the robotic population from the tumor region in Figure 1(c). The simulation successfully models targeted drug delivery using chemotaxis, with robots accumulating in the tumor region due to binding and chemoattractant gradients.

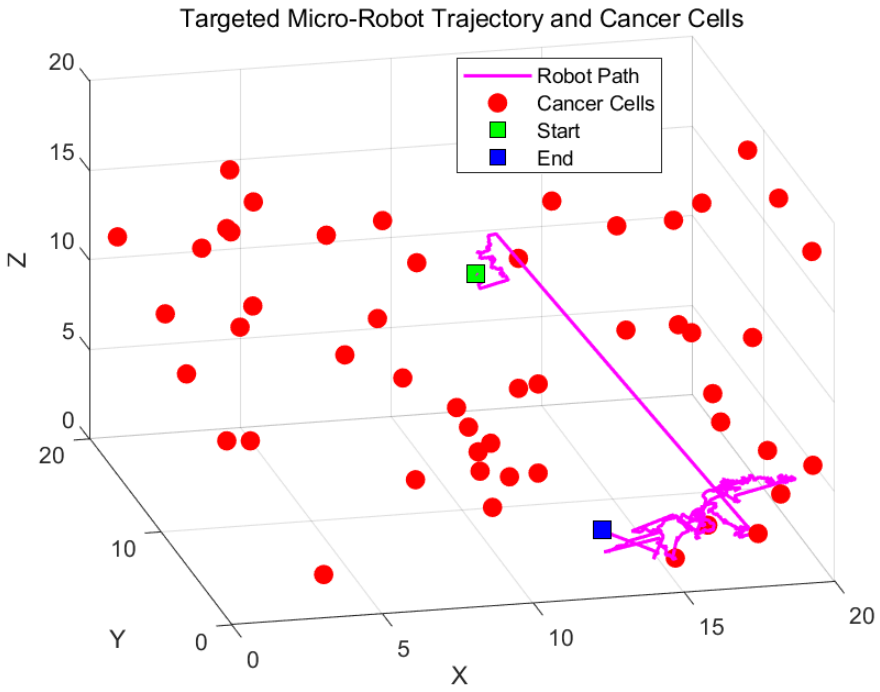

Figure 2:

Figure 2 clearly shows the robot's path, cell positions, and start/end points with appropriate markers and labels.

(a)

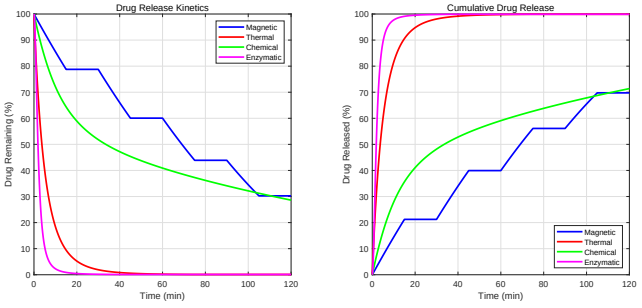

(b)

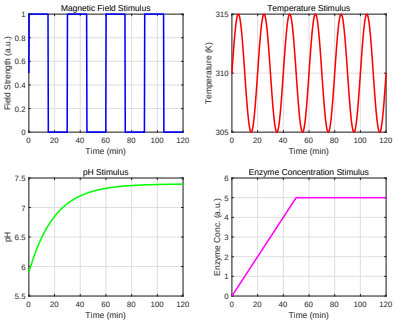

Figure 3: A comprehensive view for stimuli-responsive drug release from micro-robots: (a) ; (b) .

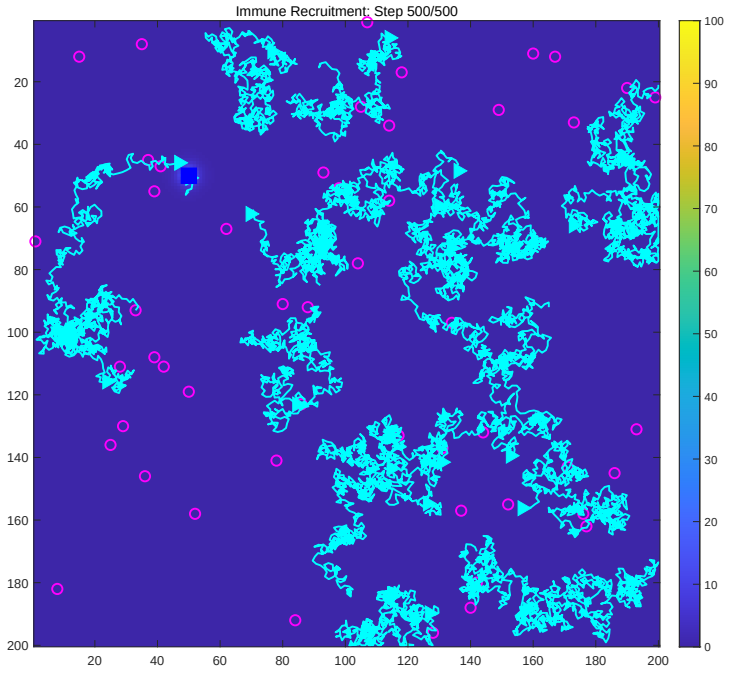

Figure 4:

4. Conclusions and future challenges

Such studies are currently in progress and will be reported in future publications.

References

References